Probing the ionization wave packet and recollision dynamics with an elliptically polarized strong laser field in the nondipole regime

J. Maurer,[1,*] B. Willenberg,[1] J. Daněk,[2] B. W. Mayer,[1] C. R. Phillips,[1] L. Gallmann,[1] M. Klaiber,[2] K. Z. Hatsagortsyan,[2,†] C. H. Keitel,[2] and U. Keller[1]

[1]*Department of Physics, ETH Zurich, 8093 Zurich, Switzerland*

[2]*Max-Planck-Institut für Kernphysik, Saupfercheckweg 1, 69117 Heidelberg, Germany*

(Received 7 April 2017; published 10 January 2018)

We explore ionization and rescattering in strong mid-infrared laser fields in the nondipole regime over the full range of polarization ellipticity. In three-dimensional photoelectron momentum distributions (3D PMDs) measured with velocity map imaging spectroscopy, we observe the appearance of a sharp ridge structure along the major polarization axis. Within a certain range of ellipticity, the electrons in this ridge are clearly separated from the two lobes that commonly appear in the PMD with elliptically polarized laser fields. In contrast to the well-known lobes of direct electrons, the sharp ridge is created by Coulomb focusing of the softly recolliding electrons. These ridge electrons are directly related to a counterintuitive shift of the PMD peak opposite to the laser beam propagation direction when the dipole approximation breaks down. The ellipticity-dependent 3D PMDs give access to different ionization and recollision dynamics with appropriate filters in the momentum space. For example, we can extract information about the spread of the initial wave packet and the Coulomb momentum transfer of the rescattering electrons.

DOI: 10.1103/PhysRevA.97.013404

I. INTRODUCTION

Rescattering of the photoelectron with the parent ion in strong laser fields is an important concept [1]. It is the basis for high harmonic generation (HHG) [2,3] and for attosecond science [4,5]. Further applications include time-resolved photoelectron holography [6] and molecular imaging [7]. In particular, rescattering in strong mid-infrared (mid-IR) laser fields is interesting because of the high photoelectron energies. These high energies allow for HHG even with keV photon energies [8] and increase the resolution in imaging experiments [9]. For mid-IR fields, the high electron velocities reached in the long-wavelength regime [10,11] cause the magnetic $\mathbf{v} \times \mathbf{B}$ term of the Lorentz force to become significant. This is a signature of the breakdown of the dipole approximation: In this regime, the vector potential can no longer be assumed as spatially homogeneous and the laser magnetic field needs to be included [12–16]. For linear polarization, the additional interplay with the magnetic laser field and the Coulomb potential during rescattering with the parent ion shifts the peak of the projected photoelectron momentum distributions (PMDs) opposite to the beam propagation direction [17]. Another feature discovered for mid-IR strong-field ionization in linearly polarized laser fields are caustic structures in PMDs, such as "low-energy structures" (LESs) of different orders [18–24]. The appearance of the low-energy peaks in the PMD were explained by longitudinal bunching of tunneled electrons during slow recollisions [25–31] on a background of Coulomb-focused (CF) electrons [32,33]. Recollisions exist also in a laser field of elliptical polarization [34–38]; however, in this case caustics in PMDs have not yet been observed.

Coulomb focusing and the related caustic structures due to multiple recollisions of electrons [39–41] carry important information on the rescattering dynamics [42–48]. These dynamics have not been observed in experiments so far, because the rescattered electrons are embedded within a large background of direct photoelectrons.

In this paper, we experimentally separate these rescattered electrons from the background of direct electrons. For that, we measure three-dimensional photoelectron momentum distributions (3D PMDs) over the full range of polarization ellipticity using a xenon gas target and strong mid-IR fields. Within a certain range of ellipticity we discovered an initially unexpected ridge structure in between the well-known lobe structure (Fig. 1). We can show that these ridge electrons are created by Coulomb focusing of electrons that rescatter with the parent ion. The Coulomb focusing is significantly affected by the magnetic laser field interaction. In contrast, the two lobes contain the direct electrons which did not experience any rescattering with the parent ion. This separation allows us to experimentally isolate the rescattered electrons in momentum space and to directly study the rescattered photoelectrons.

We therefore can extract information about the width of the ionized electron wave packet and the momentum transfer due to the Coulomb interaction with the atomic core during the recollisions. This information is beneficial for all recollision-based methods of attosecond spectroscopy [6,7,9,49,50]. We also show that the electrons in the ridge are directly related to the counterintuitive shift of the peak position of the complete projected PMD along the laser beam propagation direction caused by the combined effects of the magnetic laser field and the Coulomb forces of the parent ion in the nondipole regime [17].

*jocmaure@phys.ethz.ch
†k.hatsagortsyan@mpi-k.de

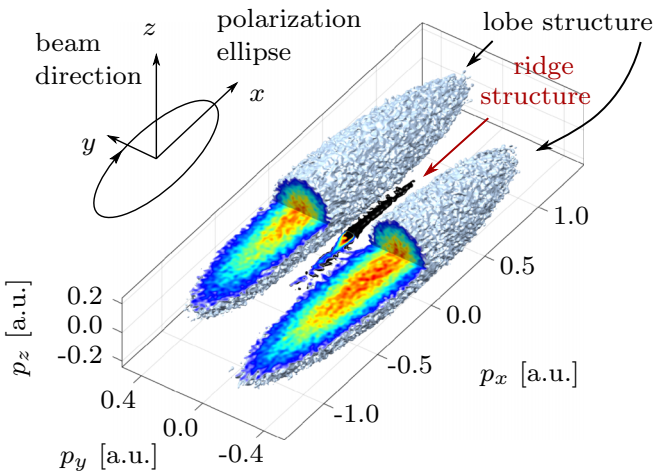

FIG. 1. Reconstructed isosurface of a 3D PMD with a partial cut in the polarization plane (p_x, p_y). The 3D PMD is produced by a mid-IR laser pulse with a center wavelength of 3.4 μm, a pulse length of 50 fs, a peak intensity of 6×10^{13} W/cm^2, and an ellipticity of $\epsilon = 0.11$. The ridge structure (which is due to rescattering of ionized electrons with the parent ion) around $p_y = 0$ is clearly separated from the common main lobes (which are due to direct electrons).

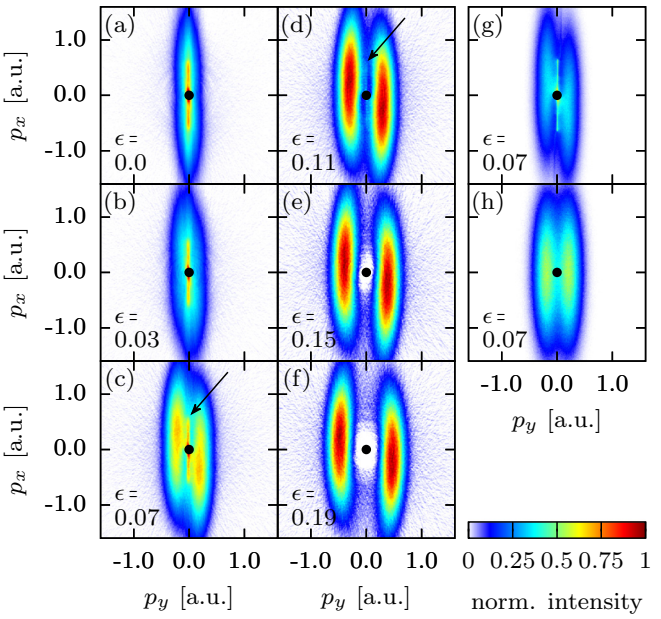

FIG. 2. PMDs in the polarization plane measured at a peak intensity of 6×10^{13} W/cm^2 for the ellipticities 0, 0.03, 0.07, 0.11, 0.15, 0.19, in (a) to (f), respectively. The central spot stemming from Rydberg states was covered by a black dot for illustration purposes [51,52]. The PMDs shown are projections from the range $|p_z| < 0.06$ a.u. onto the polarization plane. These PMDs reveal a sharp line structure for ellipticities of $\epsilon = 0.07$ and $\epsilon = 0.11$ (indicated by black arrow) that disappears for larger ellipticity. Corresponding classical trajectory Monte-Carlo (CTMC) calculations with $\epsilon = 0.07$ are shown in (g) and (h). In (h), the Coulomb potential is neglected for the CTMC calculation, and no ridge structure is visible.

We demonstrate experimentally that this shift transitions from negative (i.e., against to the laser beam propagation direction) at small ellipticities to positive values at higher ellipticities.

II. EXPERIMENTAL DETAILS

We measured the PMDs with a velocity map imaging spectrometer (VMIS) [53–56]. The target gas, xenon, was ionized by an OPCPA system that delivers few-cycle pulses at a center wavelength of 3.4 μm [57,58] that are focused into the interaction region.

In this paper, we use a coordinate scheme based on the polarization ellipse of the laser beam: the coordinate z denotes the direction of the laser propagation, x the major and y the minor polarization axes (Fig. 1). p_x, p_y, and p_z denote the corresponding electron momenta.

To obtain the full 3D PMD, we used a tomographic reconstruction scheme [38,59,60]. Here the 2D momentum images were recorded by the VMIS in a plane containing the beam propagation direction z. From a set of 2D PMDs versus angle, p_x and p_y components of the 3D PMD are reconstructed (see Appendix B).

III. RESULTS

We recorded 3D PMDs at various ellipticities and an intensity of 6×10^{13} W/cm^2 with 50-fs pulses. A reconstructed 3D PMD from a measurement with an ellipticity of $\epsilon = 0.11$ is visualized as an isosurface in Fig. 1. The isosurface exhibits two main lobes and a sharp ridge around $p_y = 0$.

In Fig. 2 we show projections of the 3D PMDs onto the polarization plane (p_x, p_y) for several ellipticities. For the projections, we used a momentum filter of $|p_z| < 0.06$ a.u.. With increasing ellipticity, the ellipsoidally shaped PMD evolves into two well-known lobes [61–63] on the short axis of the polarization ellipse [64]. The maxima are rotated by approximately 90° with respect to the maximum of the electric field, with small but significant deviations from 90° due to the Coulomb interaction of the electron with the parent ion [62,65,66], ionization delay times [61–63], and multielectron effects [66].

In these polarization plane projections, one observes the appearance of the sharp, thin ridge around $p_y = 0$ for small ellipticities, in particular for $\epsilon = 0.07$ and $\epsilon = 0.11$. The ridge is indicated by arrows in Figs. 2(c) and 2(d). We compare our experimental results with classical trajectory Monte Carlo (CTMC) simulations using the two-step model of strong-field ionization with both electric and magnetic field components included [17,66]. The initial conditions for the photoelectrons are obtained from adiabatic tunnel ionization theory in parabolic coordinates [66–70], while the subsequent electron dynamics in the laser pulse and the Coulomb potential of the parent ion is treated classically. These semiclassical simulations reproduce the appearance of the ridge. We performed CTMC simulations with [Fig. 2(g)] and without [Fig. 2(h)] the Coulomb potential included. These simulations clearly show that the Coulomb potential is indeed required to reproduce the ridge in the measured PMDs.

Next, we discuss how the magnetic field effects influence the PMD ridge in the laser propagation direction z (Fig. 3). The ellipticity was varied from linear to close-to-circular ($\epsilon = 0.97$) for a constant peak power and pulse duration. This approach keeps the total momentum transfer per cycle from the

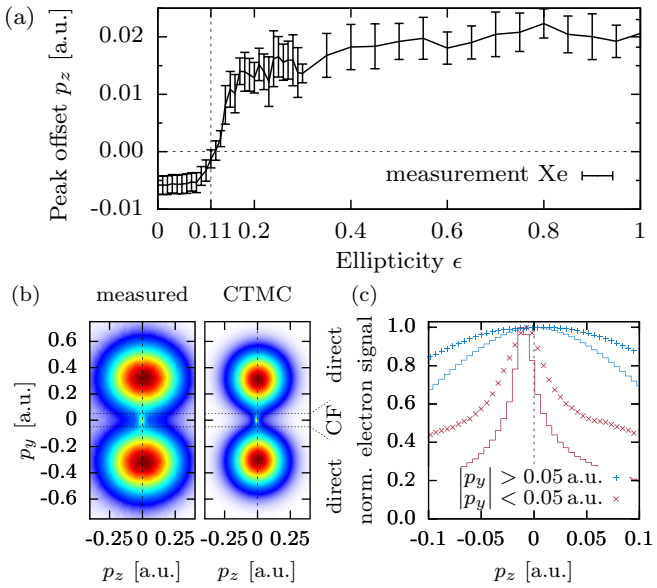

FIG. 3. (a) p_z position of the peak of the complete projection of the measured PMDs onto the beam propagation axis (p_z) as a function of ellipticity for constant intensity. We observe a transition from negative to positive values of p_z with a zero crossing at $\epsilon \approx 0.12$. (b) Projection of a complete reconstructed 3D PMD recorded at a peak intensity of 6×10^{13} W/cm^2 and an ellipticity of $\epsilon = 0.11$ together with the corresponding result from CTMC simulations. The sharp line structure is clearly visible around $p_y = 0$. (c) Projections of the PMD onto the beam propagation axis (p_z) for direct electrons (blue marker, with filter $|p_y| > 0.05$ a.u. applied) and CF electrons (red marker, with filter $|p_y| < 0.05$ a.u. applied) together with the corresponding result from CTMC simulations (solid). The peak of the CF electrons is shifted opposite to the beam propagation direction, whereas the direct electrons are shifted in beam propagation direction.

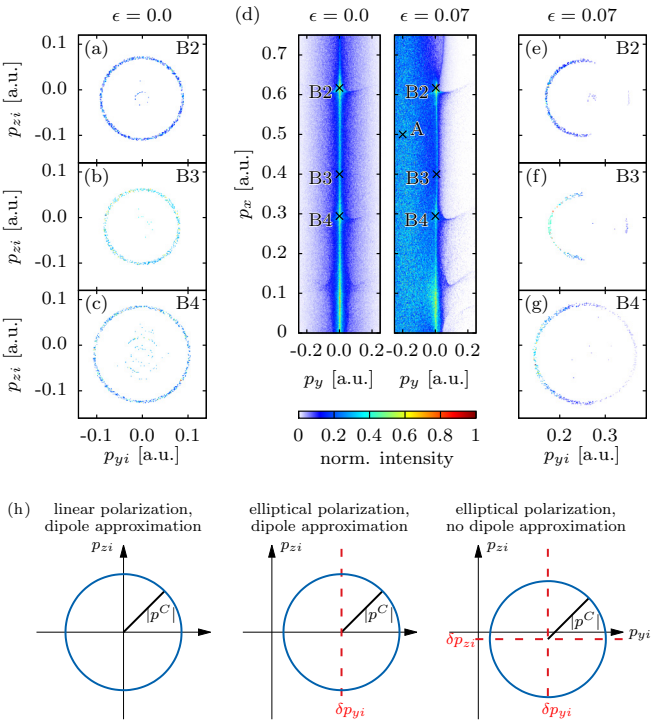

FIG. 4. CTMC calculations for electrons that originate within the central half cycle of the pulse. The central figures (d) show the ridge region for two ellipticities $\epsilon = 0$ (left) and for $\epsilon = 0.07$ (right). We show the PMDs projected over the range $|p_z| < 0.06$ a.u. Characteristic points *Bn* indicate trajectories with *n* recollisions with the parent ion. The sharp ridge is visible as a line through the points *Bn*. Panels (a)–(c) and (e)–(g) show the initial conditions for the trajectories having final momenta near points *B*2 (a) and (e), *B*3 (b) and (f), and *B*4 (c) and (g). The final momentum is within a $(0.01)^3$ a.u. bin around the points *Bn*: $p_x(B2) = 0.61$, $p_x(B3) = 0.44$, $p_x(B4) = 0.29$. Note that there is a positive offset in p_{yi} of the structures in the right column, which arises due to the ellipticity. The additional offset in the p_{zi} direction is caused by the combined influence of the magnetic field and the Coulomb potential. (h) Schematic of the different contributions to the shift of the ring of the initial momenta with respect to the linear case in dipole approximation. The ellipticity induces a shift of δp_{yi} in p_y direction whereas the nondipole effects induce a shift in the p_z direction of δp_{zi}. $|\mathbf{p}^C|$ denotes the Coulomb momentum transfer upon recollision.

field onto a free electron independent of the ellipticity. For each ellipticity step, photoelectron momentum images in the (p_x, p_z) plane were recorded. The complete PMDs were projected onto the beam propagation axis, the peak position along the p_z coordinate was determined and plotted as a function of the ellipticity [Fig. 3(a)]. We observe an increase of the peak position with increasing ellipticity from negative values (i.e., opposite to the beam propagation direction) to positive values (i.e., in beam propagation direction) with a zero crossing at an ellipticity of $\epsilon \approx 0.12$.

We will show next that this counterintuitive shift opposite to the beam propagation direction is directly related to the ridge in the 3D PMD. We are able to experimentally isolate the rescattering electrons undergoing Coulomb focusing by choosing a narrow momentum range of $|p_y| \leqslant 0.05$ a.u. from the 3D PMD recorded at an ellipticity of $\epsilon = 0.11$ [Figs. 3(b) and 3(c)]. The electrons inside and outside this range are projected separately onto the p_z axis [Fig. 3(c)]. A central spot stemming from ionization of Rydberg atoms was removed prior to the projections by ignoring all electrons with $|\mathbf{p}| < 0.03$ a.u. [51,52] (see Appendix B). We observe that only the position of the peak from CF electrons lies at a negative value of p_z. Increasing the ellipticity supresses rescattering and thus, the PMD and its projection becomes dominated by electrons that interact only weakly with the Coulomb potential of the parent ion. However, for ellipticities $\epsilon \lesssim 0.12$, the sharp ridge dominates the projection of the full PMD onto the p_z axis. As a result, we observe in this case a peak that is shifted opposite to beam propagation direction via the interplay between the Coulomb potential and the magnetic laser field [17].

As shown in Figs. 2 and 3 and discussed above we can explain the ridge structure with our CTMC simulations. We therefore can gain more insight into the electron dynamics that leads to the creation of the ridge. We start with the simpler case of linear polarization ($\epsilon = 0$) and relate this to our results with elliptical polarization ($\epsilon = 0.07$). For that, we analyze the initial momentum conditions of the photoelectrons that end within the ridge (Fig. 4). For this analysis, we choose characteristic points on the ridge where electrons accumulate in the final PMD. These points, denoted *Bn*, are marked by crosses

in the (p_x, p_y) plane in Fig. 4(d). Here n indicates the number of recollisions that the electron underwent during the ionization process. The electrons at $B2$ and $B4$ underwent at least one slow recollision. A slow recollision corresponds to the case when the momentum p_x vanishes at the moment of recollision [27]. The initial momentum distributions are obtained from trajectories that end in a $(0.01\ \text{a.u.})^3$ sized bin around the characteristic points in the final momentum space. The ridge at $p_y \approx 0$ is created due to Coulomb focusing of these initial momentum distributions (left and right panels in Fig. 4).

In a linearly polarized laser field, the electrons contributing to the ridge appear with a nonvanishing (p_{yi}, p_{zi}) momentum at the tunnel exit and end up with a vanishing (p_y, p_z) momentum after propagation. This means the Coulomb potential focuses the initial ring-shaped momentum distribution in the (p_{yi}, p_{zi}) plane [Fig. 4(a)–4(c)] into close-to-zero momentum in p_y and p_z for linear polarization. Therefore the radius of this initial PMD ring is an indicator for the strength of Coulomb momentum transfer at rescattering, denoted by $|\mathbf{p}^C|$.

In the case of elliptical polarization with small ellipticity, the radii of the rings in the initial (p_{yi}, p_{zi})-momentum space [Figs. 4(e)–4(g)] are nearly the same as in the linear polarization case. In fact, one can show that the same recollision dynamics (same Coulomb momentum transfer due to the same recollision parameters) for elliptical polarization can be achieved, if the electron starts at the tunnel exit with a momentum offset with respect to the linear polarization case (see Appendix A for details)

$$\begin{aligned}\delta p_{yi} &= \frac{\epsilon E_0}{\omega}\cos\eta_i,\\ \delta p_{zi} &= -\int_{\eta_i}^{\eta_r}\left\{\frac{[\mathbf{A}(\eta)-\mathbf{A}\eta_i)]^2}{2c}+\frac{\mathbf{p}_i^{(\epsilon)}}{c}\cdot[\mathbf{A}(\eta)-\mathbf{A}(\eta_i)]\right\}\\ &\quad\times\frac{d\eta}{\eta_r-\eta_i},\end{aligned} \tag{1}$$

with the peak electric field E_0, angular frequency ω, vector potential $\mathbf{A}(\eta)$, and the ionization and recollision phases η_i, η_r, respectively. This is the reason for the shift of the center of the rings of the initial momentum distribution (p_{yi}, p_{zi}) in Fig. 4. The situation is schematically illustrated in Fig. 4(h). Further, we can provide a quantitative estimate for the final momentum of the CF electrons, taking into account the momentum offset for recolliding electrons induced by the ellipticity and nondipole drift (Appendix A):

$$\begin{aligned}p_{yf} &\approx 0,\\ p_{zf} &= -\int_{\eta_i}^{\eta_r}\left[\frac{\mathbf{A}^2(\eta)}{2c}+\left(\mathbf{p}_i^{(\epsilon)}-\mathbf{A}(\eta_i)\right)\cdot\frac{\mathbf{A}(\eta)}{c}\right]\frac{d\eta}{\eta_r-\eta_i},\end{aligned} \tag{2}$$

where the latter is the electron average drift momentum between the ionization and the recollision. The p_z component of the rescattered electrons is negative, while for the direct electrons it is positive, in full agreement with the experimental observation.

Our analysis unveils the relation of the ridge structure that we observed with elliptical polarization with the LES. Slow recollisions cause the horizontal caustic lines in Fig. 4(d). These horizontal caustic structures are the cause for peaks that are observed in LESs on a background of CF electrons. The same radii of the rings and the same p_x position of the horizontal caustics caused by slow recollisions for elliptical and linear polarization are an indicator for the similarity of the recollision dynamics that lead to the LES and the ridge structure. At an intermediate point $B3$, the electron undergoes not exactly a slow recollision. As a result, the initial momentum ring is more distorted than for $B2$ and $B4$ in the linear polarization case. Nevertheless, also in this case there is similar Coulomb focusing dynamics occurring, as indicated by the similarity of the ring radii in Figs. 4(b) and 4(f).

We can also estimate the Coulomb momentum transfer p^C at recollision from our measurements. This momentum transfer can be extracted from the ellipticity at which the side lobes start to separate from the ridge in the PMD (Fig. 2). In this case, Coulomb focusing is not strong enough anymore, and the final momentum $p_{yf} \approx \epsilon E_0/\omega$ is larger than the Coulomb momentum transfer (i.e., $\epsilon E_0/\omega \gtrsim p^C$). In our experiment the lobes start to separate at an ellipticity between 0.03 and 0.07 as seen in Figs. 2(b) and 2(c). This allows us to experimentally determine the average Coulomb momentum transfer to be within a range of $p_C \approx 0.09$–0.22 a.u.. This range is in agreement with the corresponding radii of the momentum space rings in Fig. 4.

Next, we extract information about the initial momentum spread of the wave packet. According to adiabatic tunnel ionization theory, the momentum-dependent ionization rate is described by a Gaussian centered around zero with a 2σ width of $\Delta_\perp^{PPT} = \sqrt{2E_0}/(2I_p)^{1/4}$. If the ellipticity is increased, the initial momenta of the ridge electrons are shifted in p_y direction [Fig. 4(h)]. Once this shift exceeds the width of the initial wave packet, we expect the ridge to disappear. From the crossover of the projected PMD peak [Fig. 3(a)], we know that the ridge does indeed disappear for ellipticities $\epsilon \gtrsim 0.12$. We estimate the width of the initial wave packet with the ellipticity-dependent momentum displacement $\Delta_\perp = \Delta p_y \approx \epsilon E_0/\omega \approx 0.37$ a.u.. This value is slightly larger than one expects from tunnel ionization theory, $\Delta_\perp^{PPT} = 0.30$ a.u.. From the wave packet spread $\Delta_\perp^{PPT} \propto I_p^{-1/4}$ we expect only a weak dependence of our results on the atomic species (see Appendix B).

However, we cannot expect an exact prediction of this threshold because CTMC calculations based on tunnel ionization theory also predict a smaller final PMD [Fig. 3(b)] due to a narrower initial momentum spread. This could be due to multielectron effects on the ionization of xenon atoms [71]. Moreover, we can estimate the spatial extent of the returning wave packet via the corresponding recollision coordinate of the most probable electron trajectory. At the turnover ellipticity of $\epsilon = 0.12$, it can be obtained via the Simple Man's model: $\Delta y_r \approx \epsilon E_0/\omega^2 \approx 28$ a.u., which is much larger than the radius of a xenon atom that is on the order of 2–4 a.u..

IV. CONCLUSION

In conclusion, we have experimentally separated the rescattered CF electrons from the large background of direct photoelectrons in the 3D PMD by using elliptically polarized mid-IR pulses. We showed that these separated rescattered electrons accumulate on a clearly visible PMD ridge structure along the

major polarization axis that also contains the electrons that underwent slow recollisions. We concluded that this ridge has the same origin as LESs. We used the nondipole response of that ridge to obtain estimates of the initial momentum spread as well as the spatial extend of returning the electron wave packet. Furthermore, we provided an estimate of the momentum transfer from the Coulomb field on the electron upon recollision that is in agreement with the result from our theoretical analysis. Information about the ionization wave packet is important for HHG spectroscopy [49], tomographic orbital imaging [50], and momentum transfer onto the electron upon recollison $|\mathbf{p}^C|$ is important for recollision-based photoelectron imaging methods such as photoelectron holography [6] and photoelectron self-diffraction [7].

ACKNOWLEDGMENTS

This research was supported by the NCCR MUST, funded by the Swiss National Science Foundation and by the ERC advanced grant ERC-2012-ADG_20120216 within the seventh framework programme of the European Union. B.W. was supported by an ETH Research Grant ETH-11 15-1.

APPENDIX A: THEORY

1. Coulomb focusing with elliptical polarization

The ridge structure of recolliding electrons originates from a contraction in momentum transverse to the major polarization axis. In a linearly polarized laser field, the electrons contributing to the ridge are ionized with a nonvanishing transverse momentum at the tunnel exit and appear after propagation with a vanishing transverse momentum. Their initial distribution is a ring in the (p_{yi}, p_{zi})-initial momentum distribution; see Fig. 4. In the case of a linearly polarized laser field, the electrons which are initially (i.e., at the tunnel exit) distributed inside this ring obtain a large momentum transfer during recollisions and end up outside of the chosen final momentum bin near the vanishing transverse momentum without caustics.

In the case of the elliptically polarized laser field, there are two modifications to this picture. For small ellipticities the rescattering and Coulomb focusing, similar to the case of linear polarization, takes place for electrons which initially are distributed in a *shifted* ring of initial momenta in the (p_{yi}, p_{zi}) plane. The radius of the ring of the initial momentum space distribution is an indicator for Coulomb focusing. It is nearly the same for linear and elliptical polarization, i.e., Coulomb momentum transfer for these trajectories is qualitatively the same.

The points $B2$ and $B4$ in Fig. 4 corresponding to the slow recollision condition do not change their position in the PMD when changing ellipticity, which is due to the similarity of the underlying trajectories. Next, we analyze these trajectories analytically to show that the recollision parameters are similar for linear and elliptical polarization up to a certain value of ellipticity. Furthermore, we calculate the final momentum of the recolliding electrons. The points $B2$ and $B4$ are particularly suitable for our analysis. Outside these points along the ridge the ellipticity of the field acts as a small perturbation and does not influence our main conclusions.

2. Trajectories of recolliding electrons in an elliptically polarized laser field

The trajectory of a recolliding electron is obtained from the solution of the classical equations of motion in an elliptically polarized laser field, treating the Coulomb field effect as a perturbation which affects the electron trajectory near the tunnel exit and at recollisions.

The electric field of the laser field is

$$E_x = E_0 \cos\eta, \quad E_y = \epsilon E_0 \sin\eta, \tag{A1}$$

with the phase of the laser field $\eta = \omega(t - z/c)$, the ellipticity $0 \leqslant \epsilon \leqslant 1$, the laser field amplitude E_0, the frequency ω, and the speed of light c. The envelope of the pulse is neglected. Atomic units are used throughout.

For the electron dynamics in the plane laser field the canonical momentum in the polarization plane is conserved:

$$p_x - A_x(\eta) = \text{const}, \quad p_y - A_y(\eta) = \text{const}, \tag{A2}$$

with the electron kinetic momentum components $p_{x,y}$ in the polarization plane, and the laser vector potential $\mathbf{A}(\eta) = (A_x(\eta), A_y(\eta), 0)$:

$$A_x(\eta) = -\frac{E_0}{\omega}\sin\eta, \quad A_y(\eta) = \epsilon\frac{E_0}{\omega}\cos\eta. \tag{A3}$$

The electron momentum in the laser polarization plane after the ionization is

$$p_x = -\frac{E_0}{\omega}(\sin\eta - \sin\eta_i) + p_{xi}, \tag{A4}$$

$$p_y = \epsilon\frac{E_0}{\omega}(\cos\eta - \cos\eta_i) + p_{yi}. \tag{A5}$$

where η_i is the ionization phase and $\mathbf{p}_i = (p_{xi}, p_{yi}, p_{zi})$ are the components of the initial electron momentum.

After leaving the tunnel exit a momentum transfer arises due to the Coulomb force $\delta\mathbf{p}_i^C = (\delta p_{xi}^C, \delta p_{yi}^C, \delta p_{zi}^C)$. For a simplified analysis we include this into the initial conditions of the laser-driven electron trajectories:

$$\mathbf{p}_i = \mathbf{p}_e + \delta\mathbf{p}_i^C, \tag{A6}$$

where $\mathbf{p}_e = (p_{ex}, p_{ey}, p_{ez})$ is the electron momentum at the tunnel exit. At the tunnel exit the electron momentum is transverse to the laser field polarization direction: $\mathbf{p}_{\perp e} = \mathbf{p}_e - \mathbf{p}_{\|e}$, with a vanishing component along the polarization $\mathbf{p}_{\|e} = \hat{\mathbf{e}}(\mathbf{p}_e \cdot \hat{\mathbf{e}}) = 0$. Here the laser polarization vector is

$$\hat{\mathbf{e}} = (\cos\phi, \sin\phi, 0) = \left(\frac{\cos\eta_i}{\sqrt{\cos^2\eta_i + \epsilon^2\sin^2\eta_i}}, \frac{\epsilon\sin\eta_i}{\sqrt{\cos^2\eta_i + \epsilon^2\sin^2\eta_i}}, 0\right), \tag{A7}$$

with $\tan\phi = \epsilon\tan\eta_i$.

For the electron dynamics in a plane laser field there is a third integral of motion, besides the transverse canonical momentum of Eq. (A2), due to the space-time translation symmetry:

$$\Lambda \equiv \frac{\varepsilon - cp_z}{c^2} = \text{const} \tag{A8}$$

with the electron energy $\varepsilon = c\sqrt{p_x^2 + p_y^2 + p_z^2 + c^2}$.

The electron momentum along the laser propagation direction can be found from Eq. (A8):

$$p_z = \frac{p_x^2 + p_y^2 + c^2(1-\Lambda^2)}{2c\Lambda}. \tag{A9}$$

As $c^2(1-\Lambda^2)/(2c\Lambda) = p_{zi} - (p_{xi}^2 + p_{yi}^2)/(2c\Lambda)$, we have for the longitudinal momentum

$$p_z = p_{zi} + \frac{\left(p_x^2 + p_y^2\right) - \left(p_{xi}^2 + p_{yi}^2\right)}{2c\Lambda}. \tag{A10}$$

As the ionized electron appears at the tunnel exit with a velocity much smaller than the speed of light, one has $\Lambda \approx 1 - p_{zi}/c \approx 1$, and to the order of $1/c$ the longitudinal momentum is

$$p_z \approx p_{zi} + \frac{1}{2c}[\mathbf{A}(\eta) - \mathbf{A}(\eta_i)]^2 + \frac{\mathbf{p}_i}{c} \cdot [\mathbf{A}(\eta) - \mathbf{A}(\eta_i)]. \tag{A11}$$

From Eqs. (A4), (A5), and (A11), the electron relativistic equations of motion in the laser field read

$$\Lambda\omega\frac{dx}{d\eta} = -\frac{E_0}{\omega}(\sin\eta - \sin\eta_i) + p_{xi}, \tag{A12}$$

$$\Lambda\omega\frac{dy}{d\eta} = \epsilon\frac{E_0}{\omega}(\cos\eta - \cos\eta_i) + p_{yi}, \tag{A13}$$

$$\Lambda\omega\frac{dz}{d\eta} = \frac{1}{2c}[\mathbf{A}(\eta) - \mathbf{A}(\eta_i)]^2 + \frac{\mathbf{p}_i}{c} \cdot [\mathbf{A}(\eta) - \mathbf{A}(\eta_i)] + p_{zi}, \tag{A14}$$

which is derived using the relation $(\varepsilon/c^2)d\eta/dt = \omega\Lambda$. The solution of the latter is

$$x = \frac{E_0}{\omega^2}(\cos\eta - \cos\eta_i) + \left[p_{xi} + \frac{E_0}{\omega}\sin\eta_i\right]\frac{(\eta - \eta_i)}{\omega} + x_i, \tag{A15}$$

$$y = \epsilon\frac{E_0}{\omega^2}(\sin\eta - \sin\eta_i) + \left[p_{yi} - \epsilon\frac{E_0}{\omega}\cos\eta_i\right]\frac{(\eta - \eta_i)}{\omega} + y_i, \tag{A16}$$

$$z = \frac{1}{2c}\int_{\eta_i}^{\eta}[\mathbf{A}(\eta') - \mathbf{A}(\eta_i)]^2\frac{d\eta'}{\omega} + p_{zi}\frac{(\eta - \eta_i)}{\omega} + z_i + \frac{1}{c}\int_{\eta_i}^{\eta}\mathbf{p}_i \cdot [\mathbf{A}(\eta') - \mathbf{A}(\eta_i)]\frac{d\eta'}{\omega}, \tag{A17}$$

where the initial coordinates at the ionization phase η_i correspond to the tunnel exit:

$$\begin{aligned} x_i &\approx -\frac{I_p E_x(\eta_i)}{E^2(\eta_i)} = -\frac{I_p}{E_0}\frac{\cos\eta_i}{\cos^2\eta_i + \epsilon\sin^2\eta_i}, \\ y_i &\approx -\frac{I_p E_y(\eta_i)}{E^2(\eta_i)} = -\frac{I_p}{E_0}\frac{\epsilon\sin\eta_i}{\cos^2\eta_i + \epsilon\sin^2\eta_i}, \\ z_i &\approx 0. \end{aligned} \tag{A18}$$

3. Recollisions in an elliptically polarized laser field

Recollisions can happen not only in a linearly polarized laser field but also in a laser field of elliptical polarization. We derive the conditions under which the recollision dynamics (recollision parameters) for elliptical polarization are similar to those in the case of a linear polarization within dipole approximation.

a. Linear polarization within dipole approximation

Let us consider an electron contributing to the ridge structure in the case of linear polarization and dipole approximation, when the final transverse momentum of the electron is vanishing:

$$p_{yf}^{(0)} \approx p_{zf}^{(0)} \approx 0. \tag{A19}$$

The electron contributing to the ridge structure with an initial momentum $\mathbf{p}_i = (p_{xi}^{(0)}, p_{yi}^{(0)}, p_{zi}^{(0)})$ has the following recollision coordinates:

$$x_r^{(0)} = 0, \tag{A20}$$

$$y_r^{(0)} = p_{yi}^{(0)}\frac{\eta_r - \eta_i}{\omega}, \tag{A21}$$

$$z_r^{(0)} = p_{zi}^{(0)}\frac{\eta_r - \eta_i}{\omega}, \tag{A22}$$

where η_r is the recollision phase, and Eq. (A20) defines the recollision. The momentum transfer upon recollision due to the Coulomb field is $\delta\mathbf{p}_r^{C(0)}$, and the final transverse momentum of the electron is vanishing in the case of linear polarization when it ends up at the ridge:

$$\begin{aligned} p_{yf}^{(0)} &= p_{yi}^{(0)} + \delta p_{yr}^{C(0)} = 0, \\ p_{zf}^{(0)} &= p_{zi}^{(0)} + \delta p_{yr}^{C(0)} = 0. \end{aligned} \tag{A23}$$

Consequently, the initial momentum components transverse to the laser polarization are determined by the Coulomb momentum transfer at the recollision:

$$p_{yi}^{(0)} = -\delta p_{yr}^{C(0)}, \quad p_{zi}^{(0)} = -\delta p_{zr}^{C(0)}. \tag{A24}$$

b. Elliptical polarization with nondipole treatment

According to Eq. (A16), the electron transverse coordinates (with respect to the major axis of the polarization ellipse) at the recollision in the case of elliptical polarization is

$$y_r^{(\epsilon)} = \epsilon\frac{E_0}{\omega^2}(\sin\eta_r - \sin\eta_i) + \left(p_{yi}^{(\epsilon)} - \epsilon\frac{E_0}{\omega}\cos\eta_i\right)\frac{(\eta_r - \eta_i)}{\omega} + y_i, \tag{A25}$$

$$z_r^{(\epsilon)} = \frac{1}{2c}\int_{\eta_i}^{\eta_r}[\mathbf{A}(\eta') - \mathbf{A}(\eta_i)]^2\frac{d\eta'}{\omega} + p_{zi}^{(\epsilon)}\frac{(\eta_r - \eta_i)}{\omega} + \frac{1}{c}\int_{\eta_i}^{\eta_r}\mathbf{p}_i^{(\epsilon)} \cdot [\mathbf{A}(\eta') - \mathbf{A}(\eta_i)]\frac{d\eta'}{\omega}, \tag{A26}$$

where superscript (ϵ) indicates the case of elliptical polarization.

The recollision dynamics, i.e., the momentum transfer during recollision, in the case of elliptical polarization will be the same as in the case of linear polarization,

$$\delta p_{yr}^{C(\epsilon)} = \delta p_{yr}^{C(0)}, \quad \delta p_{zr}^{C(\epsilon)} = \delta p_{zr}^{C(0)}, \tag{A27}$$

if the impact parameter is the same

$$y_r^{(\epsilon)} = y_r^{(0)}, \quad z_r^{(\epsilon)} = z_r^{(0)}. \tag{A28}$$

The latter, using Eqs. (A21) and (A22) and (A25) and (A26), reads

$$\epsilon\frac{E_0}{\omega^2}(\sin\eta_r-\sin\eta_i)+\left[p_{yi}^{(\epsilon)}-\epsilon\frac{E_0}{\omega}\cos\eta_i\right]\frac{(\eta_r-\eta_i)}{\omega}+y_i \approx p_{yi}^{(0)}\frac{(\eta_r-\eta_i)}{\omega}, \tag{A29}$$

$$\frac{1}{2c}\int_{\eta_i}^{\eta_r}\left[\mathbf{A}(\eta')-\mathbf{A}(\eta_i)\right]^2\frac{d\eta'}{\omega}+p_{zi}^{(\epsilon)}\frac{(\eta_r-\eta_i)}{\omega} +\frac{1}{c}\int_{\eta_i}^{\eta_r}\mathbf{p}_i^{(\epsilon)}\cdot[\mathbf{A}(\eta')-\mathbf{A}(\eta_i)]\frac{d\eta'}{\omega}\approx p_{zi}^{(0)}\frac{(\eta_r-\eta_i)}{\omega}. \tag{A30}$$

We consider slow recollisions (e.g., points $B2$ and $B4$ in Fig. 4) when the longitudinal velocity is vanishing $p_{rx}=0$. This according to Eq. (A4) reads

$$\frac{E_0}{\omega}(\sin\eta_r-\sin\eta_i)=p_{xi}^{(\epsilon)}. \tag{A31}$$

Then we can derive from Eqs. (A29)–(A31)

$$p_{yi}^{(\epsilon)}=p_{yi}^{(0)}+\epsilon\frac{E_0}{\omega}\cos\eta_i-\frac{\epsilon p_{xi}^{(\epsilon)}+y_i\omega}{\eta_r-\eta_i} \approx p_{yi}^{(0)}+\epsilon\frac{E_0}{\omega}\cos\eta_i, \tag{A32}$$

$$p_{zi}^{(\epsilon)}=p_{zi}^{(0)}-\frac{1}{2c(\eta_r-\eta_i)}\int_{\eta_i}^{\eta_r}[\mathbf{A}(\eta')-\mathbf{A}(\eta_i)]^2\,d\eta' -\frac{1}{c(\eta_r-\eta_i)}\int_{\eta_i}^{\eta_r}\mathbf{p}_i^{(\epsilon)}\cdot[\mathbf{A}(\eta')-\mathbf{A}(\eta_i)]\,d\eta'. \tag{A33}$$

We estimated the last term in the first equality of Eq. (A32) to be rather small. In fact, $|p_{xi}^{(\epsilon)}|=|\delta p_{xi}^{C(\epsilon)}|\approx\pi E(\eta_i)/(2I_p)^{3/2}$, and $\eta_r-\eta_i\sim 3\pi$ at the first soft recollision, and $|\epsilon p_{xi}^{(\epsilon)}/(\eta_r-\eta_i)|\sim 10^{-3}$, at $\epsilon\sim 0.1$, $\omega=0.013$ (the laser wavelength of 3400 nm), and $E_0=0.04$ (the laser intensity of $5.8\times 10^{13}\,\mathrm{W/cm^2}$). The ratio $|y_i\omega/\epsilon p_{xi}^{(\epsilon)}|\sim\sin\eta_i$ is also small at the same values of parameters, justifying dropping the last term in the first equality of Eq. (A32).

We can conclude that the recollision dynamics in an elliptically polarized laser field is similar to the case of linear polarization with dipole approximation, if the initial momentum fulfills the conditions of Eqs. (A32) and (A33), i.e., the electrons with appropriately shifted initial momenta at the tunnel exit will create a ridge structure similar to the linear polarization.

c. Asymptotic momenta of recolliding electrons

The final momentum of the slow recolliding electrons which create the ridge structure in an elliptically polarized laser field can be found using Eqs. (A5), (A11), (A32), and (A33).

The electron momentum before the recollision is

$$p_{ry}^{(\epsilon-)}=p_{yi}^{(\epsilon)}+\epsilon\frac{E_0}{\omega}(\cos\eta_r-\cos\eta_i),$$
$$p_{rz}^{(\epsilon-)}=p_{zi}^{(\epsilon)}+\frac{1}{2c}[\mathbf{A}(\eta_r)-\mathbf{A}(\eta_i)]^2+\frac{\mathbf{p}_i}{c}\cdot[\mathbf{A}(\eta_r)-\mathbf{A}(\eta_i)]. \tag{A34}$$

The recollision induces the momentum transfer $\delta\mathbf{p}_r^{C(\epsilon)}$, and the electron momentum after the recollision is

$$p_{ry}^{(\epsilon+)}=p_{yi}^{(\epsilon)}+\delta p_{ry}^{C(\epsilon)}+\epsilon\frac{E_0}{\omega}(\cos\eta_r-\cos\eta_i),$$
$$p_{rz}^{(\epsilon+)}=p_{zi}^{(\epsilon)}+\delta p_{rz}^{C(\epsilon)}+\frac{1}{2c}[\mathbf{A}(\eta_r)-\mathbf{A}(\eta_i)]^2+\frac{\mathbf{p}_i}{c}\cdot[\mathbf{A}(\eta_r)-\mathbf{A}(\eta_i)]. \tag{A35}$$

Then the final photoelectron momentum is

$$p_{yf}^{(\epsilon)}=p_{ry}^{(\epsilon+)}-\epsilon\frac{E_0}{\omega}\cos\eta_r,$$
$$p_{zf}^{(\epsilon)}=p_{rz}^{(\epsilon+)}+\frac{\mathbf{A}^2(\eta_r)}{2c}-\frac{\mathbf{p}_r^{(\epsilon)}}{c}\cdot\mathbf{A}(\eta_r), \tag{A36}$$

which after inserting Eq. (A35) yields

$$p_{yf}^{(\epsilon)}=p_{yi}^{(\epsilon)}+\delta p_{ry}^{C(\epsilon)}-\epsilon\frac{E_0}{\omega}\cos\eta_i,$$
$$p_{zf}^{(\epsilon)}=p_{zi}^{(\epsilon)}+\delta p_{rz}^{C(\epsilon)}+\frac{\mathbf{A}^2(\eta_i)}{2c}-\frac{\mathbf{p}_i^{(\epsilon)}}{c}\cdot\mathbf{A}(\eta_i), \tag{A37}$$

where we have used that $p_{rx}=A_x(\eta_r)-A_x(\eta_i)+p_{xi}$, and $p_{ry}=A_y(\eta_r)-A_y(\eta_i)+p_{yi}$.

Now we apply the initial conditions of Eqs. (A32) and (A33), which results in

$$p_{yf}^{(\epsilon)}=p_{yi}^{(0)}+\delta p_{ry}^{C(\epsilon)},$$
$$p_{zf}^{(\epsilon)}=p_{zi}^{(0)}+\delta p_{rz}^{C(\epsilon)}+\frac{\mathbf{A}^2(\eta_i)}{2c}-\frac{\mathbf{p}_i^{(\epsilon)}}{c}\cdot\mathbf{A}(\eta_i) -\frac{1}{2c(\eta_r-\eta_i)}\int_{\eta_i}^{\eta_r}[\mathbf{A}(\eta')-\mathbf{A}(\eta_i)]^2d\eta', -\frac{1}{c(\eta_r-\eta_i)}\int_{\eta_i}^{\eta_r}\mathbf{p}_i^{(\epsilon)}\cdot[\mathbf{A}(\eta')-\mathbf{A}(\eta_i)]d\eta'. \tag{A38}$$

Taking into account the conditions of Eqs. (A24) and (A27), i.e., $\delta p_{ry,rz}^{C(\epsilon)}\approx\delta p_{ry,rz}^{C(0)}\approx p_{yi,zi}^{(0)}$, we obtain the final momentum:

$$p_{yf}^{(\epsilon)}\approx 0,$$
$$p_{zf}^{(\epsilon)}\approx-\frac{1}{\eta_r-\eta_i}\int_{\eta_i}^{\eta_r}T_z\left(\mathbf{p}_i^{(\epsilon)},\eta'\right)d\eta', \tag{A39}$$

where

$$T_z\left(\mathbf{p}_i^{(\epsilon)},\eta\right)\equiv\frac{\mathbf{A}^2(\eta)}{2c}+\left[\mathbf{p}_i^{(\epsilon)}-\mathbf{A}(\eta_i)\right]\cdot\frac{\mathbf{A}(\eta)}{c} \tag{A40}$$

is the drift momentum along the laser propagation direction.

Our conclusion from Eq. (A40) is that the ridge position for the slow recolliding electrons in the ellipically polarized laser field is not shifted along the minor axis of polarization, but it is shifted opposite the laser propagation direction by the value corresponding to the average drift momentum during the recollision.

d. Estimation of the momentum shift against the laser propagation direction

We may estimate the momentum shift against the laser propagation direction as

$$p_{zf}^{(\epsilon)} \sim -\left\{\frac{\mathbf{A}^2(\tilde{\eta})}{2c} + \left[\mathbf{p}_i^{(\epsilon)} - \mathbf{A}(\eta_i)\right] \cdot \frac{\mathbf{A}(\tilde{\eta})}{c}\right\}, \quad \text{(A41)}$$

with the effective phase $\tilde{\eta}$ during the excursion, $p_{xi}^{(\epsilon)} = \delta p_{xi}^C = \pi E_0 \cos\eta_i/(2I_p)^{3/2}$, and $p_{yi}^{(\epsilon)} - A_y(\eta_i) = \delta p_r^C$. Thus,

$$p_{zf}^{(\epsilon)} \sim -\left(\frac{E_0}{c\omega}\left\{\left[\frac{\pi E_0 \cos\eta_i}{(2I_p)^{3/2}} + \frac{E_0}{\omega}\sin\eta_i\right]\sin\tilde{\eta} + \delta p_r^C \epsilon \cos\tilde{\eta}\right\} + \frac{\mathbf{A}^2(\tilde{\eta})}{2c}\right). \quad \text{(A42)}$$

From Fig. 4 we can evaluate $\delta p_r^C \sim 0.1$, while $E_0/\omega \sim 3$, and $\pi E_0/(2I_p)^{3/2} \sim 0.1$.

For the final low longitudinal momenta $p_{xf} \to 0$, $\eta_i \to 0$, the first term in the square brackets is small, and

$$p_{zf}^{(\epsilon)} \sim -\frac{\mathbf{A}^2(\tilde{\eta})}{2c}. \quad \text{(A43)}$$

When the final momentum p_{xf} is large and rescattering is negligible, then the peak of the momentum distribution shifts along the laser propagation direction:

$$p_{zf}^{(\epsilon)} \approx \frac{\mathbf{A}^2(\eta_i)}{2c}. \quad \text{(A44)}$$

A rough estimation

$$\frac{\mathbf{A}^2(\tilde{\eta})}{2c} \sim \frac{\mathbf{A}^2(\eta_i)}{2c} \sim \frac{E_0^2}{4c\omega^2} \approx 0.017 \quad \text{(A45)}$$

fits by the order of magnitude the experimental observation shown in Fig. 3(a).

APPENDIX B: EXPERIMENT

1. General experimental details

The pulses were generated by a an optical parametric chirped-pulse amplifier (OPCPA) system that delivers few-cycle pulses at a center wavelength of 3.4 μm, a repetition rate of 50 kHz and a pulse length of 50 fs [57,58]. The laser pulses were focused by a backfocusing dielectric mirror into the interaction region.

In all experiments, we calibrated the intensity with reference measurements at close-to-circular polarization. For this calibration, the radial maximum of the torus-shaped momentum distribution was compared and calibrated against semiclassical Monte Carlo simulations [17,66].

The zero-momentum position on the detector was identified via a sharp point in the PMD recorded with linear polarization that stems from ionization of atoms that were left in a Rydberg state by the laser pulse and were subsequently ionized by the static electric field of the spectrometer [51,52]. The exact position of zero momentum in the p_z direction was determined from the projection of a small range of $p_x \leqslant 0.05$ a.u. of the PMD onto the p_z axis. This projection was fitted with a Lorentzian profile. This method was also applied to find the center in the p_y direction.

2. Reconstruction

We measured the full 3D PMD with our VMIS and a well-established tomographic reconstruction scheme. We have described this approach in more details in Ref. [56], when we transferred the attoclock technique [62,63,72] to the VMIS. The detector plane in our VMIS is horizontal in the laboratory frame, and the laser beam propagation direction is also horizontal. Therefore, individual 2D momentum images recorded by the VMIS correspond to projections of the PMD onto the horizontal plane in the laboratory frame. In order to extract a full 3D PMD, the polarization ellipse of the laser is rotated with a half-wave plate (HWP), and we record a 2D momentum image at each rotation step. At each HWP angle, the 2D PMD recorded by the VMIS corresponds to a plane containing the beam propagation direction z. By rotating the HWP, this plane is rotated around the z axis. Once this set of 2D PMDs versus angle is recorded, the full 3D PMD can be reconstructed by a tomographic scheme. The polarization is rotated in steps of two degrees. The ellipticity of the laser beam was controlled by a quarter wave plate, placed directly before the HWP. These wave plates were fully characterized via polarimetry measurements [56].

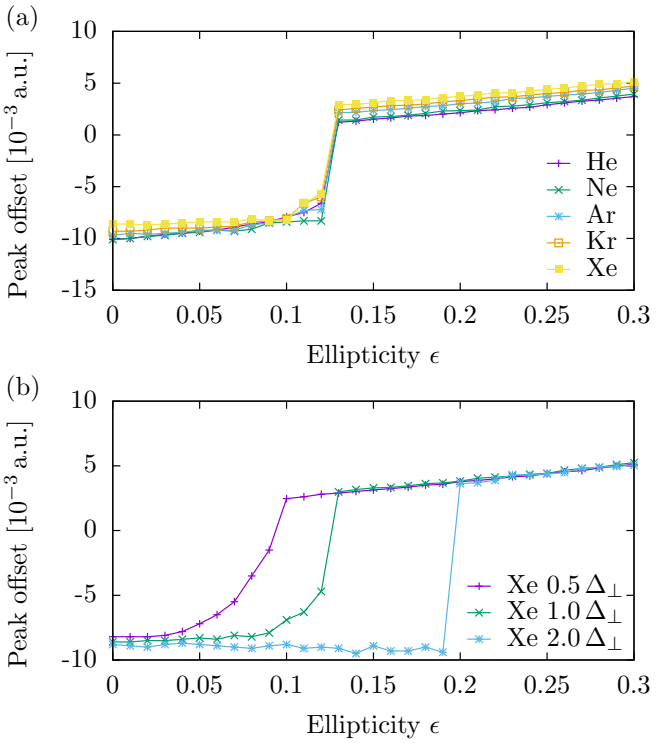

FIG. 5. Offsets of the peak of the projection of the PMDs from CTMC simulations onto the beam propagation axis (p_z) as a function of ellipticity. In (a) we show the offsets for various atomic species. The peak intensity was kept at a constant value of 6×10^{13}W/cm^2. We observe a transition from negative to positive values that is only weakly dependent on the species. In (b) we show the offsets for various momentum spreads of the initial wave packet with respect to the one expected from xenon. The results show a clear dependence of the zero transition on the momentum spread of the initial wave packet.

3. Ellipticity scan

For the ellipticity scan, the major polarization was kept parallel to the detector plane. During the measurement, we kept the intensity constant and not the peak electric field, which varies according to the ellipticity to keep the total momentum transfer per cycle from the field onto a free electron independent of the ellipticity. To extract the offset in the p_z direction, the PMDs were projected onto the beam propagation axis and the peak position was determined via a polynomial fit of the central part of the PMD (i.e., $\Delta p_z \approx 0.05$ a.u.) as a function of p_z.

We took reference measurements with linear polarization right before and after each ellipticity step to extract the zero-momentum reference.

4. Different species

According to tunnel ionization theory, the spread of the initial wave packet depends weakly on the ionization potential I_p. Thus, since our results depend on this wave packet spread, a species dependence might be observable in our data and impact our conclusions.

In order to estimate the influence of the species on our measurements, we performed simulations for different target atoms with our CTMC code [Fig. 5(a)]. We looked at the ellipticity dependence of the peak position of the projection of the complete PMD onto the p_z axis.

We observe that the zero transition, which reflects the wave packet width, is only weakly species dependent. This is consistent with the fact that the tunnel ionization theory that we use for the initial conditions of the CTMC simulation predicts a scaling of the wave packet spread with $I_p^{-1/4}$. In view of the experimental uncertainties, such a weak dependence is likely not detectable and should not affect our conclusions.

The signature of the wave packet spread in the p_z position of the zero crossing might also be affected by the I_p-dependent contributions from multiple field-oscillation cycles as well as the polarizability of the target. However, we do not expect that these contributions are significantly beyond the resolution of the simulations. Statistical fluctuations of the simulations do not allow us to determine the zero crossing with precision better than $\Delta\epsilon = \pm 0.01$.

For comparison, we also performed CTMC calculations for xenon where we varied the wave packet spread artificially [Fig. 5(b)] by a factor of two. The remaining initial parameters, ionization rate and all atomic and ionic parameters, we left unchanged. We observe a clear dependence of the p_z position of the zero crossing on the wave packet spread.

[1] P. B. Corkum, Phys. Rev. Lett. **71**, 1994 (1993).

[2] A. McPherson, G. Gibson, H. Jara, U. Johann, T. S. Luk, I. A. McIntyre, K. Boyer, and C. K. Rhodes, J. Opt. Soc. Am. B **4**, 595 (1987).

[3] M. Ferray, A. L'Huillier, X. Li, L. Lompre, G. Mainfray, and C. Manus, J. Phys. B **21**, L31 (1988).

[4] P. B. Corkum and F. Krausz, Nat. Phys. **3**, 381 (2007).

[5] F. Krausz and M. Ivanov, Rev. Mod. Phys. **81**, 163 (2009).

[6] Y. Huismans, A. Rouzée, A. Gijsbertsen, J. H. Jungmann, A. S. Smolkowska, P. S. W. M. Logman, F. Lépine, C. Cauchy, S. Zamith, T. Marchenko, J. M. Bakker, G. Berden, B. Redlich, A. F. G. van der Meer, H. G. Muller, W. Vermin, K. J. Schafer, M. Spanner, M. Y. Ivanov, O. Smirnova, D. Bauer, S. V. Popruzhenko, and M. J. J. Vrakking, Science **331**, 61 (2011).

[7] C. I. Blaga, J. L. Xu, A. D. DiChiara, E. Sistrunk, K. K. Zhang, P. Agostini, T. A. Miller, L. F. DiMauro, and C. D. Lin, Nature (London) **483**, 194 (2012).

[8] T. Popmintchev, M.-C. Chen, D. Popmintchev, P. Arpin, S. Brown, S. Ališauskas, G. Andriukaitis, T. Balčiunas, O. D. Mücke, A. Pugzlys, A. Baltuška, B. Shim, S. E. Schrauth, A. Gaeta, C. Hernández-García, L. Plaja, A. Becker, A. Jaron-Becker, M. M. Murnane, and H. C. Kapteyn, Science **336**, 1287 (2012).

[9] M. G. Pullen, B. Wolter, A.-T. Le, M. Baudisch, M. Hemmer, A. Senftleben, C. D. Schröter, J. Ullrich, R. Moshammer, C.-D. Lin, and J. Biegert, Nat. Commun. **6**, 7262 (2015).

[10] A. Di Piazza, C. Müller, K. Z. Hatsagortsyan, and C. H. Keitel, Rev. Mod. Phys. **84**, 1177 (2012).

[11] M. C. Kohler, T. Pfeifer, K. Z. Hatsagortsyan, and C. H. Keitel, in *Advances in Atomic and Molecular Physics*, Vol. 61, edited by E. A. P. Berman and C. Lin (Academic Press, Singapore, 2012), pp. 159–208.

[12] H. R. Reiss, Phys. Rev. Lett. **101**, 043002 (2008).

[13] C. H. Keitel and P. L. Knight, Phys. Rev. A **51**, 1420 (1995).

[14] M. W. Walser, C. H. Keitel, A. Scrinzi, and T. Brabec, Phys. Rev. Lett. **85**, 5082 (2000).

[15] D. B. Milošević, S. Hu, and W. Becker, Phys. Rev. A **63**, 011403 (2000).

[16] N. J. Kylstra, R. M. Potvliege, and C. J. Joachain, J. Phys. B **34**, L55 (2001).

[17] A. Ludwig, J. Maurer, B. W. Mayer, C. R. Phillips, L. Gallmann, and U. Keller, Phys. Rev. Lett. **113**, 243001 (2014).

[18] C. Blaga, F. Catoire, P. Colosimo, G. Paulus, H. Muller, P. Agostini, and L. DiMauro, Nat. Phys. **5**, 335 (2009).

[19] W. Quan, Z. Lin, M. Wu, H. Kang, H. Liu, X. Liu, J. Chen, J. Liu, X. T. He, S. G. Chen, H. Xiong, L. Guo, H. Xu, Y. Fu, Y. Cheng, and Z. Z. Xu, Phys. Rev. Lett. **103**, 093001 (2009).

[20] J. Wu, M. Meckel, S. Voss, H. Sann, M. Kunitski, L. P. H. Schmidt, A. Czasch, H. Kim, T. Jahnke, and R. Dörner, Phys. Rev. Lett. **108**, 043002 (2012).

[21] B. Wolter, M. G. Pullen, M. Baudisch, M. Sclafani, M. Hemmer, A. Senftleben, C. D. Schröter, J. Ullrich, R. Moshammer, and J. Biegert, Phys. Rev. X **5**, 021034 (2015).

[22] H. Liu, Y. Liu, L. Fu, G. Xin, D. Ye, J. Liu, X. T. He, Y. Yang, X. Liu, Y. Deng, C. Wu, and Q. Gong, Phys. Rev. Lett. **109**, 093001 (2012).

[23] J. Dura, N. Camus, A. Thai, A. Britz, M. Hemmer, M. Baudisch, A. Senftleben, C. Schröter, J. Ullrich, R. Moshammer, and J. Biegert, Sci. Rep. **3**, 2675 (2013).

[24] For caustics in electron spectra in the context of other fields of physics, we refer the reader to Ref. [26] of this article .

[25] C. Liu and K. Z. Hatsagortsyan, Phys. Rev. Lett. **105**, 113003 (2010).

[26] T.-M. Yan, S. V. Popruzhenko, M. J. J. Vrakking, and D. Bauer, Phys. Rev. Lett. **105**, 253002 (2010).

[27] A. Kästner, U. Saalmann, and J. M. Rost, Phys. Rev. Lett. **108**, 033201 (2012).

[28] C. Lemell, K. I. Dimitriou, X.-M. Tong, S. Nagele, D. V. Kartashov, J. Burgdörfer, and S. Gräfe, Phys. Rev. A **85**, 011403 (2012).

[29] M. Möller, F. Meyer, A. M. Sayler, G. G. Paulus, M. F. Kling, B. E. Schmidt, W. Becker, and D. B. Milošević, Phys. Rev. A **90**, 023412 (2014).

[30] S. A. Kelvich, W. Becker, and S. P. Goreslavski, Phys. Rev. A **93**, 033411 (2016).

[31] E. Diesen, U. Saalmann, M. Richter, M. Kunitski, R. Dörner, and J. M. Rost, Phys. Rev. Lett. **116**, 143006 (2016).

[32] T. Brabec, M. Y. Ivanov, and P. B. Corkum, Phys. Rev. A **54**, R2551 (1996).

[33] D. Comtois, D. Zeidler, H. Pepin, J. C. Kieffer, D. M. Villeneuve, and P. B. Corkum, J. Phys. B **38**, 1923 (2005).

[34] N. I. Shvetsov-Shilovski, S. P. Goreslavski, S. V. Popruzhenko, and W. Becker, Phys. Rev. A **77**, 063405 (2008).

[35] X. Wang and J. H. Eberly, Phys. Rev. Lett. **103**, 103007 (2009).

[36] F. Mauger, C. Chandre, and T. Uzer, Phys. Rev. Lett. **105**, 083002 (2010).

[37] C. Liu and K. Z. Hatsagortsyan, Phys. Rev. A **85**, 023413 (2012).

[38] D. Dimitrovski, J. Maurer, H. Stapelfeldt, and L. B. Madsen, Phys. Rev. Lett. **113**, 103005 (2014).

[39] K. Sasaki, X. M. Tong, and N. Toshima, J. Phys. B **42**, 165603 (2009).

[40] C. Huang, Q. Liao, Y. Zhou, and P. Lu, Opt. Expr. **18**, 14293 (2010).

[41] C. Liu and K. Z. Hatsagortsyan, J. Phys. B **44**, 095402 (2011).

[42] L. Guo, S. S. Han, X. Liu, Y. Cheng, Z. Z. Xu, J. Fan, J. Chen, S. G. Chen, W. Becker, C. I. Blaga, A. D. DiChiara, E. Sistrunk, P. Agostini, and L. F. DiMauro, Phys. Rev. Lett. **110**, 013001 (2013).

[43] B. Wolter, C. Lemell, M. Baudisch, M. G. Pullen, X.-M. Tong, M. Hemmer, A. Senftleben, C. D. Schröter, J. Ullrich, R. Moshammer, J. Biegert, and J. Burgdörfer, Phys. Rev. A **90**, 063424 (2014).

[44] Q. Z. Xia, D. F. Ye, L. B. Fu, X. Y. Han, and J. Liu, Sci. Rep. **5**, 11473 (2015).

[45] S. A. Berman, C. Chandre, and T. Uzer, Phys. Rev. A **92**, 023422 (2015).

[46] T. Keil, S. V. Popruzhenko, and D. Bauer, Phys. Rev. Lett. **117**, 243003 (2016).

[47] E. Pisanty and M. Ivanov, Phys. Rev. A **93**, 043408 (2016).

[48] J. F. Tao, Q. Z. Xia, J. Cai, L. B. Fu, and J. Liu, Phys. Rev. A **95**, 011402 (2017).

[49] H. J. Wörner, H. Niikura, J. B. Bertrand, P. B. Corkum, and D. M. Villeneuve, Phys. Rev. Lett. **102**, 103901 (2009).

[50] J. Itatani, J. Levesque, D. Zeidler, H. Niikura, H. Pépin, J.-C. Kieffer, P. B. Corkum, and D. M. Villeneuve, Nature (London) **432**, 867 (2004).

[51] T. Nubbemeyer, K. Gorling, A. Saenz, U. Eichmann, and W. Sandner, Phys. Rev. Lett. **101**, 233001 (2008).

[52] C. T. L. Smeenk, L. Arissian, B. Zhou, A. Mysyrowicz, D. M. Villeneuve, A. Staudte, and P. B. Corkum, Phys. Rev. Lett. **106**, 193002 (2011).

[53] A. T. J. B. Eppink and D. H. Parker, Rev. Sci. Instrum. **68**, 3477 (1997).

[54] D. H. Parker and A. T. J. B. Eppink, J. Chem. Phys. **107**, 2357 (1997).

[55] O. Ghafur, W. Siu, P. Johnsson, M. F. Kling, M. Drescher, and M. J. J. Vrakking, Rev. Sci. Instrum. **80**, 033110 (2009).

[56] M. Weger, J. Maurer, A. Ludwig, L. Gallmann, and U. Keller, Opt. Expr. **21**, 21981 (2013).

[57] B. W. Mayer, C. R. Phillips, L. Gallmann, M. M. Fejer, and U. Keller, Opt. Lett. **38**, 4265 (2013).

[58] B. W. Mayer, C. R. Phillips, L. Gallmann, and U. Keller, Opt. Expr. **22**, 20798 (2014).

[59] M. Wollenhaupt, M. Krug, J. Köhler, T. Bayer, C. Sarpe-Tudoran, and T. Baumert, Appl. Phys. B **95**, 647 (2009).

[60] C. Smeenk, L. Arissian, A. Staudte, D. Villeneuve, and P. Corkum, J. Phys. B **42**, 185402 (2009).

[61] P. Eckle, M. Smolarski, F. Schlup, J. Biegert, A. Staudte, M. Schöffler, H. G. Muller, R. Dörner, and U. Keller, Nat. Phys. **4**, 565 (2008).

[62] P. Eckle, A. N. Pfeiffer, C. Cirelli, A. Staudte, R. Dörner, H. G. Muller, M. Büttiker, and U. Keller, Science **322**, 1525 (2008).

[63] A. Landsman, M. Weger, J. Maurer, R. Boge, A. Ludwig, S. Heuser, C. Cirelli, L. Gallmann, and U. Keller, Optica **1**, 343 (2014).

[64] The two- or three-step model of strong field ionization (Simple Man's model) with purely classical propagation in the electric laser field neglecting the Coulomb potential, put forward independently by M. Yu. Kuchiev, Pis'ma Zh. Exp. Theor. Fiz. **45**, 319 (1987) [JETP Lett. **45**, 404 (1987)]; H. B. van Linden van den Heuvell and H. G. Muller, in *Multiphoton Processes*, edited by S. J. Smith and P. L. Knight (Cambridge University Press, Cambridge, 1988); T. F. Gallagher, Phys. Rev. Lett. **61**, 2304 (1988); K. J. Schafer, B. Yang, L. F. DiMauro, and K. C. Kulander, *ibid.* **70**, 1599 (1993).

[65] M. Bashkansky, P. H. Bucksbaum, and D. W. Schumacher, Phys. Rev. Lett. **60**, 2458 (1988).

[66] A. N. Pfeiffer, C. Cirelli, M. Smolarski, D. Dimitrovski, M. Abusamha, L. B. Madsen, and U. Keller, Nat. Phys. **8**, 76 (2012).

[67] A. M. Perelomov and V. S. Popov, Zh. Exp. Theor. Fiz. **52**, 514 (1967) [Sov. Phys. JETP **25**, 336 (1967)].

[68] M. V. Ammosov, N. B. Delone, and V. P. Krainov, Zh. Eksp. Theor. Fiz. **91**, 2008 (1986) [Sov. Phys. JETP **64**, 1191 (1986)].

[69] N. B. Delone and V. P. Krainov, J. Opt. Soc. Am. B **8**, 1207 (1991).

[70] Here, we refer to the theory of tunnel ionization in the quasistatic limit. Commonly, this case is referred to as the Ammosov-Delone-Kranov (ADK). The results of this theory are already contained in the Perelomov-Popov-Terentev (PPT) theory as the limit for a zero-frequency field.

[71] P. A. Batishchev, O. I. Tolstikhin, and T. Morishita, Phys. Rev. A **82**, 023416 (2010).

[72] C. M. Maharjan, A. S. Alnaser, X. M. Tong, B. Ulrich, P. Ranitovic, S. Ghimire, Z. Chang, I. V. Litvinyuk, and C. L. Cocke, Phys. Rev. A **72**, 041403 (2005).